Gamma rays from warm WIMP dark matter annihilation

Qiang Yuan,[1] Yixian Cao,[2] Jie Liu,[3] Peng-Fei Yin,[1] Liang Gao,[2] Xiao-Jun Bi,[1] and Xinmin Zhang[3]

[1]*Key Laboratory of Particle Astrophysics, Institute of High Energy Physics, Chinese Academy of Sciences, Beijing 100049, People's Republic of China*

[2]*Partner Group of the Max Planck Institute for Astrophysics, National Astronomical Observatories, Chinese Academy of Sciences, Beijing 100012, People's Republic of China*

[3]*Division of Theoretical Physics, Institute of High Energy Physics, Chinese Academy of Sciences, Beijing 100049, People's Republic of China*

(Received 21 July 2012; published 26 November 2012)

The weakly interacting massive particle (WIMP) often serves as a candidate for the cold dark matter. However, when produced nonthermally, it could behave like warm dark matter. In this paper, we study the properties of the γ-ray emission from annihilation of WIMP dark matter in the halo of our own Milky Way galaxy with high resolution N-body simulations of a Milky-Way-like dark matter halo, assuming a different nature of WIMPs. Due to the large free-streaming length in the scenario of warm WIMPs, the substructure content of the dark matter halo is significantly different from that of the cold WIMP counterpart, resulting in distinct predictions of the γ-ray signals from the dark matter annihilation. We illustrate these by comparing the predicted γ-ray signals from the warm WIMP annihilation to that of cold WIMPs. Pronounced differences from the subhalo sky map and statistical properties between two WIMP models are demonstrated. Due to the potentially enhanced cross section of the nonthermal production mechanism in the warm WIMP scenario, the Galactic center might be prior to the indirect detection of warm WIMPs to dwarf galaxies, which might be different from the cold dark matter scenario. As a specific example, we consider the nonthermally produced neutralino of the supersymmetric model and discuss the detectability of warm WIMPs with the Fermi γ-ray telescope.

DOI: 10.1103/PhysRevD.86.103531 PACS numbers: 95.35.+d, 95.85.Pw

I. INTRODUCTION

The so-called dark matter (DM), discovered ~80 years ago in the astronomical observations, is still one of the biggest mysteries in the fields of physics, astronomy, and cosmology. To understand the nature of DM particles is a big challenge of the community. There are several ways to detect the weakly interacting massive particle (WIMP) DM being proposed (see, e.g., Ref. [1]), among which the *indirect search* through the cosmic ray (CR) particles is the most active one in recent years due to the operation of several new-generation satellites, such as PAMELA, Fermi, and AMS02. In many kinds of CR particles, the antiparticles, γ-rays, and neutrinos are good probes to search for DM signals. Especially, γ rays are widely discussed, due to the simple propagation and the high sensitivity detections from both spatial and ground-based telescopes. The constraints on the DM parameters have become stronger and stronger in recent years thanks to the Fermi γ-ray observations [2–6].

One of the key problems in the study of the γ-ray emission from the WIMP DM annihilation is the density distribution of DM. It is observationally very difficult to determine the density distribution of DM, especailly at small scales. Currently, the postulated best knowledge about the DM density distribution comes from the numerical N-body simulations (e.g., Refs. [7–9]).

The initial matter power spectrum that describes cosmic density perturbation depends on the particle nature of DM. For the cold DM (CDM), the particle velocity when decoupling is negligible, and the corresponding free-streaming length is very short. The small free-streaming length enables structures down to very small scales to form.

The CDM scenario has been shown to be in good agreement with the observations of the cosmological large-scale structures. However, it has been a long-time problem of the CDM scenario that the expected structures are inconsistent with observations at the subgalactic scale (e.g., Refs. [10–14]). One possible solution of this problem is the warm DM (WDM) scenario (Refs. [15–17], or a recent review in Ref. [18]). In general, with a thermal distribution, the particle mass of the WDM should be as light as ~keV. After decoupling, the velocity of WDM can be fast enough to introduce a large free-streaming scale below which the structures are smoothed out. Thus, the formation of small-scale structures in the WDM scenario can be suppressed.

If the DM is finally proven to be warm, the impact on the detection of DM particles is fatal because most of these experiments aim to search for the WIMPs that are traditionally cold. For the canonical WIMPs, when produced thermally in the early Universe, the velocity is nonrelativistic after decoupling, and they behave like CDM. Alternatively, the WIMPs, if produced nonthermally, can be warm [19–22]. In Ref. [20], the authors showed explicitly that the power spectrum of these nonthermally produced WIMPs has a clear suppression at small scales. The nonthermally produced WIMP scenario will have some interesting properties for the indirect search of DM because 1) compared with the light WDM, the mass of the nonthermal WIMPs lies within the range of most high-energy CR detectors, and 2) in contrast with the thermally produced WIMPs, the annihilation cross section of nonthermal WIMPs can be larger due to the lack of direct constraints from the relic density. We will discuss the possible γ-ray signatures from such nonthermal WIMP DM annihilation in this paper.

In this paper, we focus on predicted DM annihilation signals from the Milky Way halo and its substructures based upon high resolution simulations of WDM in Ref. [23].

This paper is organized as follows. In Sec. II, we briefly introduce the picture of the nonthermally produced warm WIMPs. In Sec. III, we describe the numerical simulations used in this work and the DM density distributions for the smooth halo and subhalos according to the simulations. The signatures of γ-ray signals and detectability analysis are discussed in Sec. IV. Finally, Sec. V is the conclusion.

II. NONTHERMALLY PRODUCED WARM WIMPS

The DM particles can be nonthermally produced by the decays of topological defects such as cosmic string [19,20,24,25]. For example, we consider a model with an extra U(1) gauge symmetry that is broken by the vacuum expectation value η of a scalar field S [19]. Cosmic strings will be formed during the symmetry-breaking phase transition taking place at the temperature of $T_c \sim \eta$. After the transition, the infinite long string network coarsens, and more closed string loops form from the reconnection of the long strings. The tension of the cosmic string is determined by $\mu \sim \eta^2$. Cosmic string loops lose their energy dominantly through gravitational radiation. When the radius of a loop becomes the order of the string width, the loop will self-annihilate into its constituent field, such as scalar boson S. The DM particle χ can be produced by the decay of these heavy particles.

When the temperature of DM is higher than the freeze-out temperature $T_\chi(\sim\mathrm{O(GeV)})$, DM particles produced by cosmic string loops still keep in chemical equilibrium with standard model particles. Only the DM particles produced below T_χ will contribute to the nonthermal DM relic density Ω_{NT}. It is found that the nonthermal DM is mostly contributed by the loops decaying at T_χ [Eq. (A2)]. Therefore, the DM production process does not affect the big bang nucleosynthesis results. Through adjusting the model parameters, the relic density of DM can also be naturally explained (for more details, see Appendix A).

In such a scenario, DM particle χ may carry large initial momentum p_c due to the decay of the heavy particle. p_c can be written as $p_c = \alpha T_c$ where α is a numerical factor determined by a detailed model. Here, we define a typical variable $r_c = a(t)p(t)/m_\chi$ which is a constant during the cosmic evolution [20]. If we choose the cosmic scale factor at the present time $a(t_0) = 1$, r_c can be understood as today's velocity of the DM particles if there is no structure formation. The comoving free-streaming scale R_f is given by [20]

$$R_f = \int_{t_i}^{t_{\mathrm{EQ}}} \frac{v(t')}{a(t')} \mathrm{d}t' \sim 2r_c t_{\mathrm{EQ}}(1+z_{\mathrm{EQ}})^2 \times \ln\left[\sqrt{1+\frac{1}{r_c^2(1+z_{\mathrm{EQ}})^2}} + \frac{1}{r_c(1+z_{\mathrm{EQ}})}\right], \quad (1)$$

where "EQ" denotes the radiation-matter equality.

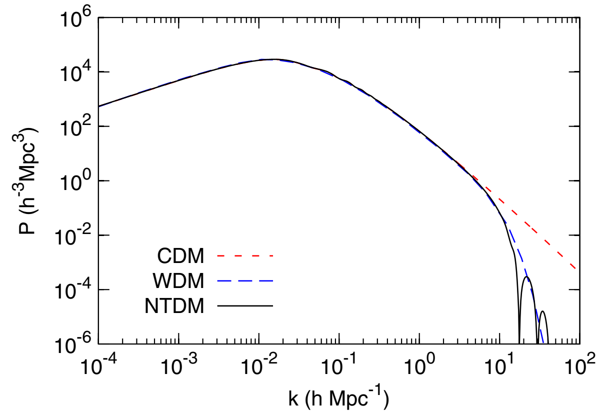

FIG. 1 (color online). Linear matter power spectra of CDM (red, short-dashed lines), canonical light WDM (blue, long-dashed lines) and nonthermal warm WIMP (black, solid lines).

The free streaming of DM particles will imprint on the late-time structure formation. This effect can be simply seen by the matter power spectrum of DM. We use a modified version of CAMB[1] [26] to calculate the matter power spectrum of the nonthermally produced DM scenario, shown in Fig. 1. Here, we adopt $r_c = 10^{-7}$. Note the mass of the nonthermal DM does not explicitly affect the calculation of the power spectrum because its effect can be cancelled by the initial momentum (see the definition of r_c). For comparison, the power spectra for CDM and the canonical light WDM are also shown. The power spectrum of the canonical WDM corresponds to a sterile neutrino with mass $\sim$2 keV, which is also the input power spectrum of the N-body simulation (see below in Sec. III). We can see that a clear suppression of the power at small scales appears both for the light WDM and the warm WIMP scenarios. The free-streaming property makes the nonthermal DM behave similarly with WDM. Due to the similarity of the input power spectra of the light WDM and nonthermal warm WIMPs, we use the simulation results for the light WDM in the following discussion of the indirect detection of warm WIMPs.

[1] http://camb.info

III. NUMERICAL SIMULATION RESULTS

In this section, we describe briefly numerical simulations used in this work and present the properties of the DM distribution based on the numerical simulations. The simulations used in this study are two matched ultrahigh resolution simulations of a Milky-Way-sized DM halos run with different natures of DM models but with the otherwise same numerical setup as well as cosmological parameters. For the CDM simulation, we use "Aq-A-2", from the *Aquarius* Project [7]. In order to facilitate comparison of DM annihilation emission from cold and warm DM models, for the same halo, we further performed a high-resolution simulation assuming a WDM model by using the same phase in the initial density field as that of the Aq-A-2 simulation but a different matter spectrum matching a particular WDM model. In the numerical calculation of this paper, we adopt a 2 KeV sterile neutrino [27] as our WDM model which lies within the bound of the $Ly\alpha$ constraint [27]. The chosen WDM introduces a cutoff emerging at a wave number $k \sim 10h$ Mpc^{-1} in the initial matter power spectrum, below which the power spectrum is well consistent with that of CDM [23]. In the scenario of nonthermal WIMPs, such as a heavy particle S decaying into two WIMPs χ, for χ around 100 GeV, it requires the mass of particle S around 10^8 GeV [20]. In our simulation, the mass of the "particle" is 1.37×10^4 M$_\odot$, and the number of particles is larger than 100 million within r_{200}, the radius inside which the mean DM density is 200 times the critical density. Therefore, the lowest-mass subhalos resolved in our simulation are 3×10^5 M$_\odot$ if requiring more than 20 particles for a subhalo. The total mass within r_{200} of the halo is about 1.8×10^{12} M$_\odot$. See Table 1 of Ref. [23] for the basic information of the simulations. For a more detailed description of our simulation, please refer to Ref. [23].

A. Smooth halo

The density profile of the smooth component of the simulated halo of the CDM simulation was analyzed in Ref. [28]. It was shown that the smooth halo density profile can be well fitted with an Einasto profile [29]

$$\rho(r) = \rho_{-2} \exp\left[-\frac{2}{\alpha}\left(\left(\frac{r}{r_{-2}}\right)^{\alpha} - 1\right)\right], \qquad (2)$$

where $\rho_{-2} \approx 0.14$ GeV cm^{-3}, $r_{-2} \approx 15.7$ kpc, and $\alpha \approx 0.17$ [28]. The local density of DM is then given as $\rho_\odot \approx 0.44$ GeV cm^{-3} at $R_\odot = 8.5$ kpc. A higher local density compared with the canonical 0.3 GeV cm^{-3} was also found in recent studies [30–32].

For the WDM halo, the density profile of the smooth halo is essentially the same as that of CDM down to the numerical resolution limit of our simulation [33]. The expectation that a core may appear in the center of the halo for WDM due to phase space density constraint [34–36] is not clearly seen in the simulation; this is because the core size of the Milky-Way-sized halo is predicted to be smaller than the resolution limit of our simulation and thus is not resolved. It was shown recently that a density core was indeed observed in WDM simulations, at a scale smaller than 100 pc for 1–2 keV WDM and halo mass 10^8–10^{10} M$_\odot$ [37]. For the Milky-Way-like halo, the expected core will be even smaller, and the halo density profile will be indistinguishable from that of the CDM halo, within the precision of subdegree of the present γ-ray detectors. In this work, we adopt the same equation (2) to describe the density profile of the smooth halo for WDM.

B. Subhalos

Based on the simulation results, we find 20529 gravitational bounded subhalos for CDM simulation and 219 subhalos for WDM[2] simulation within the virial radius of the main halo. The minimum mass of the resolved subhalo is found to be $\sim 3 \times 10^5$ M$_\odot$, and the maximum mass is about 10^{10} M$_\odot$.

We define the annihilation luminosity of a subhalo as $L_i = \int \rho_i^2 dV_i$. In the work, we adopt the Navarro-Frenk-White (NFW, Ref. [39]) profile for the subhalos. The determination of the parameters of the NFW density profile from the simulated circular velocity profile can be found in the appendix of Ref. [39]. For WDM subhalos, we employ a constant density core with size $r_c \approx 0.03 \times (\frac{\sigma}{\mathrm{km\,s^{-1}}})^{-0.5}$ kpc, where σ is the velocity dispersion of the subhalo [40]. Beyond r_c, the density distribution is identical with the NFW profile. The γ-ray flux from DM annihilation of this subhalo is then proportional to L_i/d_i^2, with d_i the distance of the subhalo from Earth. To calculate d_i of each subhalo, a random location of the solar system that is 8.5 kpc away from the halo center is chosen.

The mass-luminosity and mass-flux scattering plots of the subhalos are shown in Fig. 2. From the mass-flux relation, we see that, in general, subhalos in the CDM case are brighter than that of WDM because of a relatively lower concentration of subhalos in WDM compared to CDM [23]. There are also fewer subhalos of WDM which can have comparable fluxes to that of CDM. Especially, we find the most massive subhalos are usually not the brightest objects. The subhalos with masses 10^7–10^9 M$_\odot$ have larger probability to give high fluxes [41].

For the CDM case, it is expected that there should be a large number of unresolved substructures below the resolution limit of the simulation, which can extend to a mass comparable to or even lower than that of the Earth, 10^{-6} M$_\odot$ [42,43]. To include the contribution of unresolved subhalos, we have to extrapolate the subhalos to lower mass, according to the statistical properties of the

[2]Note, for WDM case, the number of subhalos might be overestimated due to the numerical fragmentation of filaments [38].

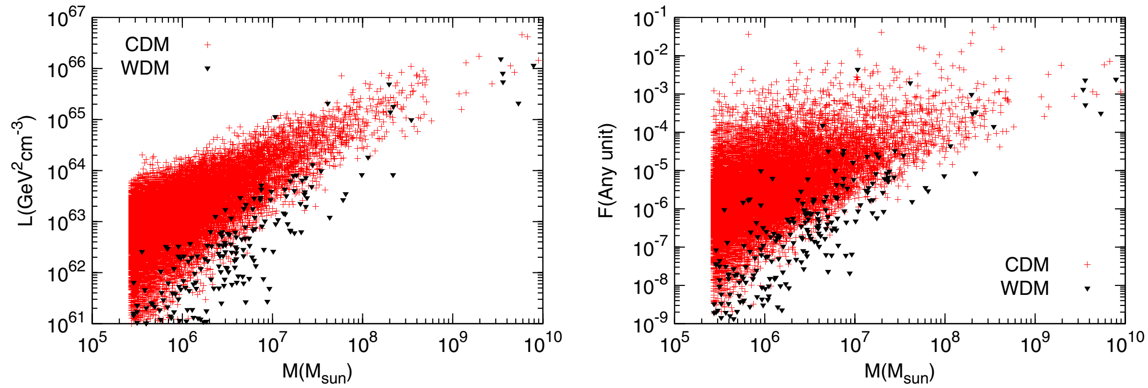

FIG. 2 (color online). Annihilation luminosity (L, left) and relative flux (F, right) versus mass of subhalos for CDM and WDM simulations.

resolved subhalo distributions [7,44]. We present the basic statistical results of the subhalos of CDM and WDM based on the simulations in Appendix B. For the WDM case, because free-streaming length of the chosen WDM particle is as large as 200 kpc, the smallest dark matter halo expected to form in the model is, therefore, about 2.5×10^9 $M_\odot$ [17], corresponding to $\sim 10^5$ particles in our simulation, and hence is well resolved in our simulation. Thus, we believe that our WDM simulation has resolved all subhalos and, therefore, has no unresolved subhalo component. There are some spurious subhalos formed in our simulation via artificial fragmentation of filaments as noted by Ref. [38]; however, we expect that contribution to the annihilation luminosity due to these spurious subhalos is small because of their low abundance. We do not consider them in the following analysis.

C. *J* factors

The γ-ray flux observed at the Earth from DM annihilation can be written as

$$\phi_\gamma(E_\gamma, \psi) = \frac{\rho_\odot^2 R_\odot}{4\pi} \frac{\langle\sigma v\rangle}{2m_\chi^2} \frac{\mathrm{d}N}{\mathrm{d}E_\gamma} \times J(\psi), \quad (3)$$

where m_χ is the mass of the DM particle, $\langle\sigma v\rangle$ is the annihilation cross section weighted with the velocity of the DM particle, and $\frac{\mathrm{d}N}{\mathrm{d}E_\gamma}$ is the γ-ray yield spectrum per annihilation. The dimensionless astrophysical J factor, related to the DM density profile, is defined as

$$J(\psi) = \frac{1}{\rho_\odot^2 R_\odot} \int_{\mathrm{LOS}} \rho^2(l)\mathrm{d}l, \quad (4)$$

where ψ is defined as the angle between the observational direction and the Galactic center direction for the observer at Earth. The integral is done along the line of sight (LOS). Taking the detector's angular resolution into account, the J factor for a resolved subhalo is defined as

$$J_{\mathrm{sub}}^i(\psi) = \frac{1}{\rho_\odot^2 R_\odot} \frac{L_i}{d_i^2} \times \frac{1}{2\pi\sigma^2} \exp\left[-\frac{(\psi - \psi_i)^2}{2\sigma^2}\right], \quad (5)$$

where L_i, d_i, and ψ_i are the luminosity, distance, and central direction of the ith halo. The exponential term on the right-hand side corresponds to a Gaussian smooth with width σ.

Based on the numerical simulation of WDM, we calculate the J factor of the smooth halo and the subhalos. The sky maps of the J factors of the smooth halo, resolved subhalos, and the total result for WDM are shown in Fig. 3. The color bar shows the value of $\log(J)$. For resolved subhalos, we employ Gaussian smoothing with $\sigma = 0.5°$.

The sky maps of the CDM subhalos based on the simulation Aquarius has been given in Ref. [8]. To compare with the sky map of WDM subhalos given in this work, we have also shown the sky maps of CDM in Appendix B (see Fig. 10). From those two figures, we can clearly see the differences between the CDM and WDM annihilation signals from subhalos. For CDM, there is a non-negligible diffuse component from the unresolved subhalos, especially at the directions far away from the Galactic center. The number of the potentially visible subhalos above the diffuse component is much higher for CDM than WDM. There is also difference in the Galactic center due to the expected presence of a core in the WDM scenario. However, we may overestimate the size of the core in this work compared with that found in the simulations [37]. The actual difference may be smaller.

The accumulative subhalo number, which represents the subhalos with J factor greater than some value J_{sub} versus J_{sub}, is shown in Fig. 4. The different lines in each group represent the random choice of the location of the solar system in the halo, with distance fixed to be 8.5 kpc from the center. We can see that the number distribution of WDM is flatter than that of CDM. This is because in the CDM case, the relative weight of smaller subhalos compared with larger ones is higher than that in the WDM case. The property presented in Fig. 4, if detectable, is useful to probe the nature of the DM particles.

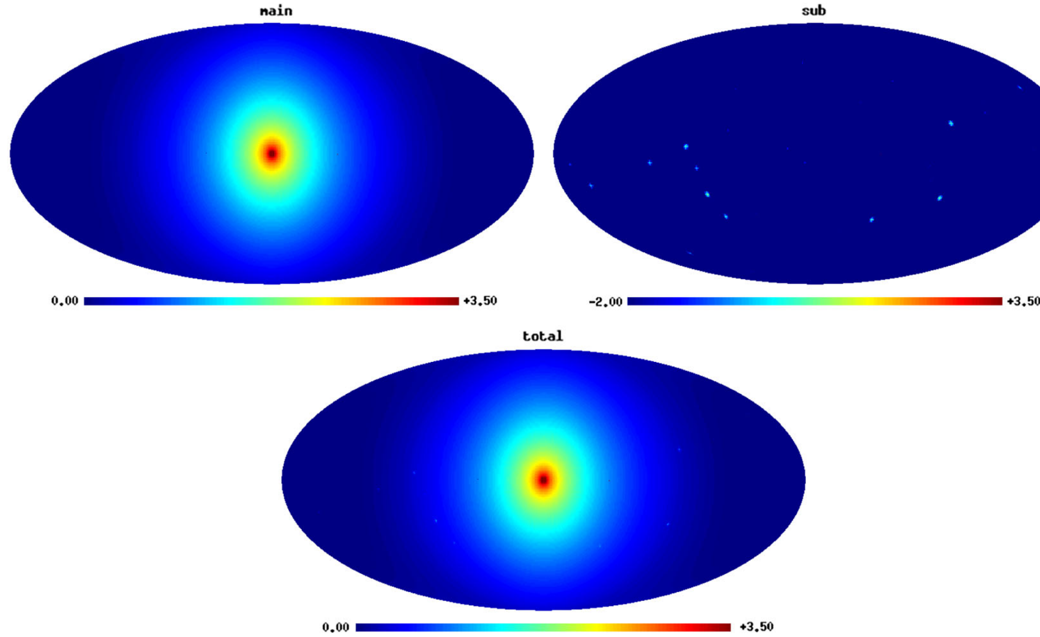

FIG. 3 (color online). Sky maps of the J factors of the main halo (top left), resolved subhalos (top right), and total contribution (bottom) for WDM.

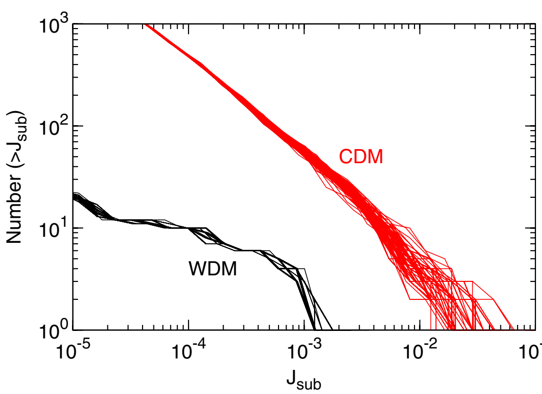

FIG. 4 (color online). Accumulative number versus J of subhalos.

IV. GAMMA-RAY SIGNALS

In this section, we study the γ-ray signals from the warm WIMP annihilation. We will present the astrophysical γ-ray background and the detectability of the γ rays from warm WIMP annihilation by Fermi.

A. Benchmark models of supersymmetric DM

For the warm WIMP, the annihilation cross section may be larger than that of cold WIMPs, which are constrained by the relic density of DM. However, considering the constraints from, e.g., γ rays and antiprotons, the cross section cannot be arbitrarily large. The constraint from PAMELA antiproton data showed that the allowed boost factor[3] of neutralinolike DM should be less than 10 for $O(100)$ GeV DM [45]. The new constraints from Fermi observations of dwarf galaxies also gave an allowed boost factor of several for $O(100)$ GeV DM [5]. Taking the above constraints on the WIMP annihilation cross section into account, we give two explicit benchmark models to realize the cold and warm WIMP scenarios in supersymmetric DM models.

In the supersymmetric (SUSY) theory with R-parity conservation, the lightest neutralino, which is the combination of gaugino and Higgsino, is a well motivated candidate of DM [46]. In general, there are four parameter regions to obtain the correct thermal relic density of a neutralino: (1) all the sfermions are light, neutralinos annihilate via t-channel sfermion exchange; (2) neutralinos scatter with sfermions with nearly mass degeneracy which is so-called "coannihilation"; (3) $\tilde{\chi}_1^0$ has significant component of Higgsino or wino, with the main annihilation channel to heavy gauge boson or Higgs; (4) neutralinos annihilate via s-channel Higgs resonance with $2m_{\tilde{\chi}_1^0} \sim m_{A^0}$, or m_{h^0}, m_{H^0}. In the first region, the light sfermions are stringently constrained by recent LHC results [47,48]. In the coannihilation region, the neutralino annihilation cross section is often much smaller than the "natural value" $3 \times 10^{-26}\ \mathrm{cm^3\,s^{-1}}$. Thus, it is difficult to observe the products of DM annihilation in indirect detections. In the third region, neutralino annihilation could produce a large flux of γ rays due to a cascade decay of gauge

[3]Defined as $\langle \sigma v \rangle / 3 \times 10^{-26}\ \mathrm{cm^3\,s^{-1}}$.

TABLE I. Relevant parameters for the two benchmark models. The unit of m_0, m_{H_u}, m_{H_d}, $m_{1/2}$, A_0, $m_{\tilde{\chi}_1^0}$ is GeV, and of $\langle\sigma v\rangle$ is $\mathrm{cm^3\,s^{-1}}$.

	m_0	m_{H_u}	m_{H_d}	$m_{1/2}$	A_0	$\tan\beta$	sign(μ)	$m_{\tilde{\chi}_1^0}$	$\langle\sigma v\rangle$
Warm WIMP	1200	1300	788	500	-1000	40	+	211	2.70×10^{-25}
Cold WIMP	1200	1300	824	500	-1000	40	+	211	1.38×10^{-26}

bosons or Higgs. However, a significant component of Higgsinos or winos in the neutralino might induce a large interaction between DM and the nucleon, which is stringently constrained by recent direct detections, such as XENON100 [49].

Here, we consider two benchmark models in the "Higgs funnel" region as the cold and warm WIMP candidates. The DM annihilation is enhanced by s-channel pseudoscalar Higgs exchange with resonance effect $m_{A^0}\sim 2m_{\tilde{\chi}_1^0}$, and the main final states of DM annihilations are $b\bar{b}$.[4] The ATLAS and CMS collaborations have discovered a 125 GeV Higgs-like boson [50,51]. Because the Higgs in the minimal supersymmetric standard model is lighter than the Z boson at the tree level, it requires a large stop mass parameter or large mixing term to acquire corrected Higgs mass. It can be interpreted by some particular parameter configurations. Since here we employ the benchmark models as illustration and emphasize the difference between warm and cold WIMPs, we do not consider this issue of Higgs mass in this work.

To acquire a moderate A^0 mass easily, we consider the "nonuniversal Higgs mass" scenario [52,53], in which the Higgs mass parameters m_{H_u},m_{H_d} at the grand unified theory scale are different from other scalar masses m_0. The particle spectrum, DM thermal relic density, and annihilation cross section for the benchmark models are calculated by SuSpect [54] and micrOMEGAs [55,56] and are summarized in Table I. For the warm WIMP model adopted here, the thermal relic density of DM is $\Omega h^2_{\rm th}\sim 4.33\times10^{-3}$, much smaller than the observational value $\Omega h^2\sim 0.11$. Therefore, it must be produced via a nonthermal mechanism (see Appendix A and Ref. [24]). Given the particle models of DM, the γ-ray spectrum from the decay and fragmentation of the final-state particles is calculated using the PYTHIA simulation tool [57].

In the benchmark models, the DM parameters are $m_\chi\approx$ 211 GeV, $\langle\sigma v\rangle\approx 1.38\times10^{-26}\ \mathrm{cm\,s^{-1}}$ for cold WIMP and $2.70\times10^{-25}\ \mathrm{cm^3\,s^{-1}}$ for warm WIMP, and the annihilation final state is about $86\% b\bar{b}+14\%\tau^+\tau^-$. The cross section for warm WIMP corresponds to a boost factor of 9, which is roughly compatible with the present constraints from indirect detections. Note these constraints are applicable for neutralino DM. For other annihilation final states such as the leptons, the constraints might be different, and an even larger boost factor could be possible.

[4]The potential phenomenology problem of this region may be the large contribution to rare meson decay, such as $B_d\to X_s\gamma$ and $B_s\to\mu^+\mu^-$, due to a light pseudoscalar Higgs and a large $\tan\beta$. To avoid violating meson decay observations, some special parameters are needed to suppress total SUSY contributions from Higss sector and chargino-squark sector.

B. Astrophysical background

To discuss the detectability of DM, we have to take the astrophysical background of diffuse γ rays into account. We use the GALPROP[5] [58] code to calculate the Galactic diffuse γ-ray background. The propagation parameters adopted are $D_0=6.59\times10^{28}\ \mathrm{cm^2\,s^{-1}}$, $\delta=0.30$, $v_A=39.2\ \mathrm{km\,s^{-1}}$, and $z_h=3.9$ kpc, according to the fit to the boron-to-carbon ratio data [59]. The injection spectra of nuclei are adopted as $\gamma_1^n=1.91/\gamma_2^n=2.40$ for rigidity below/above 10 GV, which can basically reproduce the recent measurements of proton and helium spectra by PAMELA [60], as shown in Ref. [61]. Note, however, this simple injection model may not well describe the detailed hardening structures of the CR spectra above several hundred GV, or the difference between proton and helium spectra ([60,62,63]). For CR electrons, the injection spectra are $\gamma_1^e=1.50/\gamma_2^e=2.56$ for rigidity below/above 3.55 GV as derived according to the pure background fit to the newest e^+e^- data [61]. Such a pure background component cannot explain the e^+e^- excesses revealed by several experiments [64–68]. As illustrated in Ref. [69], the contribution to the total diffuse γ rays from the extra astrophysical sources of e^+e^-, e.g., pulsars, is always negligible in all regions of the sky. For the purpose of the current study, we think it is enough to employ such a rough background model. Finally, the extra-Galactic γ-ray background is adopted to be the Fermi measured results, $\phi_{\rm EG}\approx 5.89\times 10^{-7}\ (E/\mathrm{GeV})^{-2.44}\ \mathrm{cm^{-2}\,s^{-1}\,sr^{-1}\,GeV^{-1}}$ [70].

We calculate the total γ-ray sky maps for the cold and warm WIMP scenarios based on the two SUSY benchmark models given the previous subsection. The total γ-ray sky maps above 10 GeV of both the astrophysical background and the DM contribution are shown in Fig. 5. The left panel is for cold WIMPs, and the right panel is for warm WIMPs respectively. The detectability of the DM signal in presence of the astrophysical background will be discussed in the followings two subsections.

[5]http://galprop.stanford.edu/

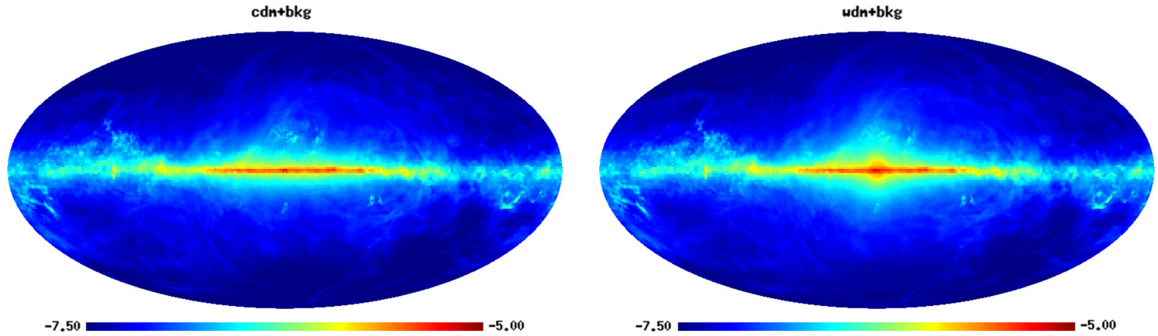

FIG. 5 (color online). Sky maps of the total γ-ray emission with background predicted by GALPROP included, for energies $E > 10$ GeV. The left panel is for the cold WIMP case, and the right panel is for the warm WIMP case.

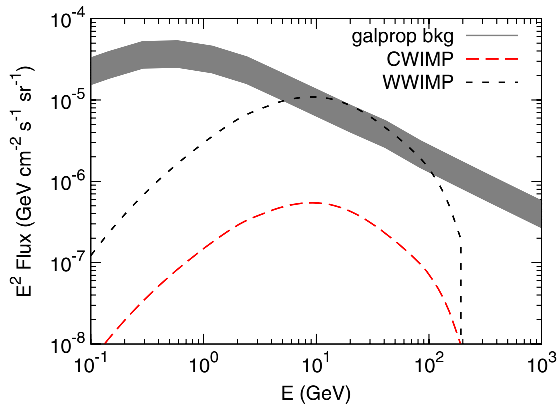

FIG. 6 (color online). Gamma-ray spectra in a $20° \times 20°$ region around the Galactic center for cold and warm WIMP scenarios. The shaded region represents the expected background of the GALPROP model (see the text).

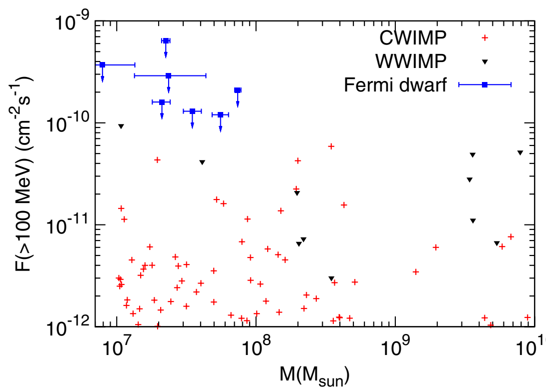

FIG. 7 (color online). Integral fluxes above 100 MeV of the DM subhalos for the cold and warm WIMP models. The arrows show the upper limits of dwarf galaxies given by Fermi observations [2].

C. Gamma rays from warm WIMP annihilation: Galactic center

Figure 6 shows the expected γ-ray spectra of the WIMP annihilation in a $20° \times 20°$ region around the Galactic center. For comparison, we also plot the calculated diffuse background described in Sec. IV B. There are all-sky survey data of diffuse γ rays from Fermi, available from the Fermi Science Support Center.[6] It was shown that the GALPROP model could reproduce the observational data within a precision of factor 2 [71]. Therefore, here, we simply employ the model results for comparison. An uncertainty of 2 times the GALPROP background is represented by the shaded region.

It is shown that for the warm WIMP scenario, we may expect a larger flux of γ rays in the Galactic center, simply due to a larger annihilation cross section of warm WIMPs. Up to now, there is no clear evidence to show the existence of signals from DM in the Fermi data.[7] However, we may expect that the warm WIMP scenario could have better detection perspective than the cold WIMP scenario.

D. Gamma rays from warm WIMP annihilation: subhalos

Finally, we discuss the detectability of DM subhalos. Figure 7 shows the integral fluxes above 100 MeV of the DM subhalos for both the cold and warm WIMP models. With a factor of $\sim$20 times larger than the cross section for the warm WIMP scenario, we can see that the fluxes of the most luminous subhalos in the two scenarios are comparable. Also shown in Fig. 7 are the upper limits (for the $80\% b\bar{b} + 20\% \tau^+\tau^-$ case) of dwarf galaxies derived through 11-month observations of Fermi [2]. The upper limits are, in general, higher than the model expected fluxes, which means the first-year Fermi data may not be able to probe the DM subhalos of both the cold and warm WIMP models discussed here.

Figure 8 gives the results of the accumulative number versus the detection significance, defined as $\sigma = N_{\rm sig}/\sqrt{N_{\rm bkg}}$, for $E > 10$ GeV and 5-yr exposure of Fermi. Here, the emission from subhalos within $\theta_{\rm half}$, angular radius containing half of the annihilation luminosity, is taken into account.

[6] http://fermi.gsfc.nasa.gov/ssc/

[7] See Ref. [72] for a claim of DM signal in the most central region of the Galactic center. However, the background and possible point source contamination need to be carefully studied.

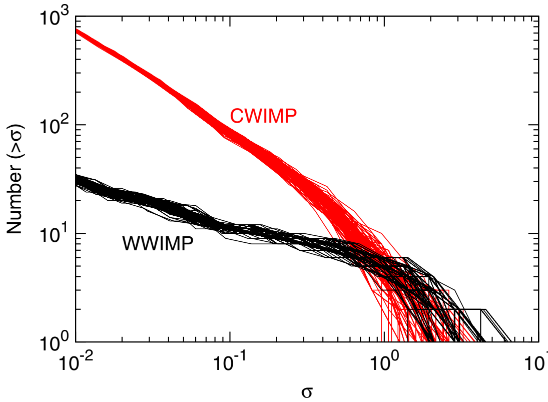

FIG. 8 (color online). The accumulative number of subhalos with significance higher than σ, for energies $E > 10$ GeV and 5-yr exposure of Fermi-LAT for the cold and warm WIMP scenarios.

The sky range to calculate the background number of events is adopted to be $\max(\theta_{\rm half}, \theta_{\rm res})$, where $\theta_{\rm res} \approx 0.1°$ is the angular resolution of Fermi-LAT at $E > 10$ GeV [73].

Similar with Fig. 4, the number distribution for warm WIMP is flatter than that for cold WIMP. This is a signature to distinguish these two scenarios. It is interesting to note that the potential detectability for warm WIMPs might be a little bit better (for high σ ones) than that of cold WIMPs, although the number of subhalos is significantly less. This is because the allowed cross section for warm WIMPs could be larger, in principle. However, it is generally difficult to detect the SUSY DM signals from subhalos with the Fermi detector, either for the cold or the warm WIMP scenarios.

V. CONCLUSIONS

Since more and more evidence shows that the DM tends to be "warm" instead of "cold" (e.g., Ref. [18]), it is necessary to investigate the possible consequence on DM detections if it is indeed warm. For the canonical light WDM particle like the sterile neutrino, most of the present DM detection experiments will be useless. Alternatively, the nonthermally produced warm WIMP scenario [19,20] might be interesting enough, for both the cosmological structure formation and the detection of DM particles. The large free streaming of the DM may help to solve the problems of the CDM scenario at the small scale, and the WIMP particles are detectable with most of the experiments searching for DM.

Based on the high-resolution numerical simulations of WDM structure formation, we study the possible γ-ray signals from the annihilation of warm WIMPs in the Milky Way. The Aquarius CDM simulations are also employed to compare with the WDM results. We investigate the expected sky maps of the DM annihilation, as well as the statistical properties of the subhalos. The detectability with the Fermi telescope is also discussed for two benchmark SUSY models of warm and cold WIMP scenarios, respectively. Unfortunately, we find that the detectability of the warm WIMPs with current γ-ray experiments is very poor. Nevertheless, it is interesting to investigate the theoretically expected signatures of the γ rays from warm WIMP annihilation, in case they might be detected in the future.

The major conclusions of this work can be summarized as follows.

(i) Due to a suppression of structure formation in the WDM scenario, subhalos are much less abundant in the WDM scenario, resulting in a flatter accumulative number distribution of the J factor and a different $N(>J)$ versus J relation between warm and cold WIMP models.

(ii) We find it is difficult to detect the subhalos with the Fermi telescope, both for cold and warm WIMP scenarios. It is found that the detectablity of warm WIMPs could, in principle, be better than for cold WIMPs because a moderately larger annihilation cross section is allowed for the warm WIMP scenario with a nonthermal production mechanism [24].

(iii) For an indirect WIMP search strategy, the Galactic center would likely be prior to dwarf galaxies if DM is made of warm WIMPs. For cold WIMPs, the γ-ray emission due to dark matter annihilation from the Galactic center is polluted by the high background, and the subhalos have been believed to be better targets for DM indirect searches. In the warm WIMP case, however, the emission from the Galactic center could be enhanced due to a larger cross section, while the emission from dwarf galaxies is not as significantly enhanced because of the decrease of the central DM density and concentration. For our benchmark models, the signal of the warm WIMP annihilation from the Galactic center will be ~20 times stronger than that of cold WIMPs, while it is comparable for subhalos. This might lead to a different detection strategy in case a WIMP is warm.

ACKNOWLEDGMENTS

We thank Paolo Gondolo, Shi Shao, and Charling Tao for useful discussion and the anonymous referee for helpful comments. This work is supported by National Natural Science Foundation of China under Grants No. 11075169, No. 11105155, No. 11105157, No. 11033005, No. 10975142, No. 10973018, and No. 11133003; the 973 project under Grants No. 2010CB833000, No. 2009CB24901; and Chinese Academy of Sciences under Grant No. KJCX2-EW-W01.

APPENDIX A: RELIC DENSITY OF NONTHERMAL DM FROM COSMIC STRING DECAY

Here, we briefly discuss the nonthermal DM density from cosmic string decay. We assume the correlation length scale of the string is $\xi(t)$ in the friction-dominated epoch. It can be given by $\xi(t) = \xi(t_c)(t/t_c)^{3/2}$ [74], where the initial length $\xi(t_c) \sim \lambda^{-1}\eta^{-1}$, λ is the scalar self-quartic coupling. The production of cosmic string loops induce the energy loss of long strings. The number density of loops created by long strings can be evaluated by [75,76]

$$\frac{\mathrm{d}n}{\mathrm{d}t} = \nu\xi^{-4}\frac{\mathrm{d}\xi}{\mathrm{d}t}, \tag{A1}$$

where ν is a constant of order 1. We assume each loop contributes N DM particles.

Here, we only consider the nonthermal DM particles from the decay of loops below the temperature T_χ (the corresponding time is t_chi). For $m_\chi \sim 100$ GeV, $T_\chi \sim$ GeV. Then, we can get the DM number density by integrating the redshifted cosmic string loop number density

$$n_\chi^{\mathrm{NT}}(t_0) = N\nu \int_{\xi(t_F)}^{\xi_0} \left(\frac{t}{t_0}\right)^{\frac{3}{2}} \xi^{-4}\mathrm{d}\xi, \tag{A2}$$

where t_F is the formation time of the cosmic string loops which are decaying at t_χ. Since the loop density decreases sharply with time, we can see the DM density is mainly contributed by loops that decay right after t_χ. It means most of the nonthermal DM particles are created at t_χ instantaneously.

According to the average radius of loop (formed at t_F) $R(t_F) \sim \lambda^{\frac{1}{2}} g_{t_F}^{*\frac{3}{4}} G\mu M_{pl}^{\frac{1}{2}} t_F^{\frac{3}{2}}$, and the loop shrink rate $\mathrm{d}R/\mathrm{d}t = -\Gamma G\mu$ (Γ is a constant ~10–20) [75,76], we find $t_F \sim \lambda^{-\frac{1}{3}} g_{t_F}^{*-\frac{1}{2}} \Gamma^{\frac{2}{3}} M_{pl}^{-\frac{1}{3}} t_\chi^{\frac{2}{3}}$. Then, the reduced number density of nonthermal DM particles from decays of cosmic string loops can be derived as [19,24]

$$Y_\chi^{\mathrm{NT}} = \frac{6.75}{\pi} N\nu\lambda^{\frac{3}{2}}\Gamma^{-2} g_{t_c}^{*\frac{3}{2}} g_{t_\chi}^{*} g_{t_F}^{*-\frac{5}{2}} M_{pl}^2 \frac{T_\chi^4}{T_c^6}, \tag{A3}$$

where Y_χ is defined as $Y_\chi = n_\chi/s$, $s = 2\pi^2 g_* T^3/45$ is the entropy density, and g^* is effective degrees of freedom at the corresponding time. The DM relic density is related to Y by $\Omega h^2 = 2.82 \times 10^8 Y_\chi(m_\chi/\mathrm{GeV})$. If the DM is dominated by nonthermal production, we can get the corrected DM relic density $\Omega h^2 \sim 0.11$ easily by choosing ν, $\lambda \sim 1$, $\Gamma \sim 10$, $g^* \sim 100$, $m_\chi \sim O(10^2)$ GeV, and $T_c \sim O(10^9)$ GeV [19,24].

APPENDIX B: DM DISTRIBUTION FROM AQUARIUS SIMULATION

Here, we give the statistical results used for the extrapolation of the unresolved subhalos, based on the resolved subhalos from Aquarius CDM simulations. More results can be found in Refs. [7,44].

We bin the luminosities L_i of the subhalos with respect to mass and radius. The left panel of Fig. 9 shows the differential distribution of luminosity versus subhalo mass, $\mathrm{d}L/\mathrm{d}M$, and the right panel shows the spatial distribution of the luminosity, $\mathrm{d}L/\mathrm{d}V$. When doing this analysis, we assume that $\mathrm{d}L/\mathrm{d}M$ is independent with the spatial distribution $\mathrm{d}L/\mathrm{d}V$ [8], so that we can use all the subhalos to derive both $\mathrm{d}L/\mathrm{d}M$ and $\mathrm{d}L/\mathrm{d}V$. The results for WDM are also shown in Fig. 9 for comparison.

The luminosity-mass relation $\mathrm{d}L/\mathrm{d}M$ can be fitted with a power-law function

$$\mathrm{d}L/\mathrm{d}M \propto M^{-1.14}. \tag{B1}$$

We can infer the cumulative luminosity distribution as $L(>M_{\mathrm{th}}) \propto M_{\mathrm{th}}^{-0.14} - M_{\mathrm{max}}^{-0.14}$. For $M_{\mathrm{th}} \ll M_{\mathrm{max}}$, we have $L(>M_{\mathrm{th}}) \propto M_{\mathrm{th}}^{-0.14}$. Note that this result is flatter than the mass dependence of the cumulative luminosity derived in Ref. [8] ($\propto M_{\mathrm{th}}^{-0.226}$). This may be due to the threshold effect when M_{th} is close to $M_{\mathrm{max}} \approx 10^{10}$ $\mathrm{M}_\odot$. For the

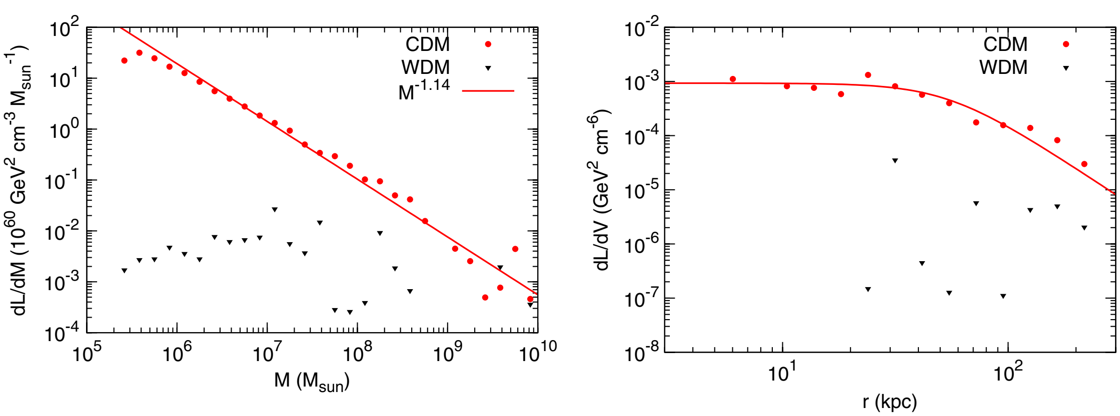

FIG. 9 (color online). Differential luminosity-mass relation $\mathrm{d}L/\mathrm{d}M$ (left) and spatial density of luminosity (right) for subhalos. Red circles are for Aq-A-2 CDM simulation, and black triangles are for Aq-AW-2 WDM simulation. Solid lines are the fitting results for CDM.

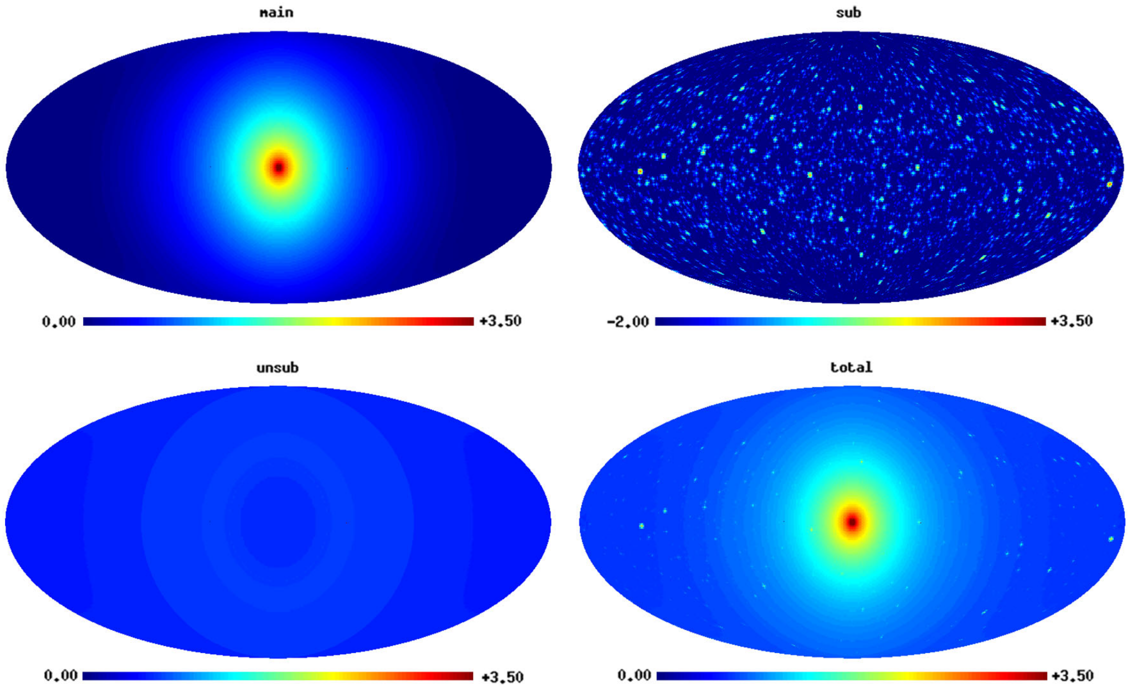

FIG. 10 (color online). Sky maps of the J factors of the smooth halo (top left), resolved subhalos (top right), unresolved subhalos (bottom left), and the total contribution (bottom right) for CDM.

spatial distribution of the luminosity $\mathrm{d}L/\mathrm{d}V$, we use an isothermal β function

$$\mathrm{d}L/\mathrm{d}V \propto \frac{1}{[1+(r/r_c)^{\beta}]} \quad \text{(B2)}$$

to fit the simulation results. The fitting parameters are $r_c \approx 54$ kpc and $\beta \approx 2.76$.

The unresolved subhalos in the CDM simulation is derived according to the fitting results of $\mathrm{d}L/\mathrm{d}M$ and $\mathrm{d}L/\mathrm{d}V$. The masses of unresolved subhalos are assumed to extend to $M_{\mathrm{min}} \approx 10^{-6}\ \mathrm{M}_{\odot}$ from $M_{\mathrm{res}} \approx 3\times 10^{5}\ \mathrm{M}_{\odot}$.

The J factor for unresolve subhalos is

$$J_{\mathrm{sub}}^{\mathrm{un}}(\psi) = \frac{1}{\rho_{\odot}^{2} R_{\odot}} \int_{\mathrm{LOS}} \left(\int_{M_{\mathrm{min}}}^{\mathrm{M_{res}}} \frac{\mathrm{d}^2 L}{\mathrm{d}M \mathrm{d}V} \mathrm{d}M \right) \mathrm{d}l. \quad \text{(B3)}$$

Figure 10 shows the sky maps of J factors of the smooth halo (top left), resolved subhalos (top right), unresolved subhalos (bottom left), and the total contribution (bottom right) for CDM. This figure is a reproduction of the result given in Ref. [8].

[1] G. Bertone, D. Hooper, and J. Silk, Phys. Rep. **405**, 279 (2005).
[2] A. A. Abdo *et al.*, Astrophys. J. **712**, 147 (2010).
[3] M. Ackermann *et al.*, J. Cosmol. Astropart. Phys. 5 (2010) 025.
[4] A. A. Abdo *et al.*, J. Cosmol. Astropart. Phys. 4 (2010) 014.
[5] M. Ackermann *et al.*, Phys. Rev. Lett. **107**, 241302 (2011).
[6] A. Geringer-Sameth and S. M. Koushiappas, Phys. Rev. Lett. **107**, 241303 (2011).
[7] V. Springel, J. Wang, M. Vogelsberger, A. Ludlow, A. Jenkins, A. Helmi, J. F. Navarro, C. S. Frenk, and S. D. M. White, Mon. Not. R. Astron. Soc. **391**, 1685 (2008).
[8] V. Springel, S. D. M. White, C. S. Frenk, J. F. Navarro, A. Jenkins, M. Vogelsberger, J. Wang, A. Ludlow, and A. Helmi, Nature (London) **456**, 73 (2008).
[9] J. Diemand, M. Kuhlen, P. Madau, M. Zemp, B. Moore, D. Potter, and J. Stadel, Nature (London) **454**, 735 (2008).
[10] B. Moore, Nature (London) **370**, 629 (1994).
[11] A. Klypin, A. V. Kravtsov, O. Valenzuela, and F. Prada, Astrophys. J. **522**, 82 (1999).
[12] A. Burkert, Astrophys. J. Lett. **447**, L25 (1995).
[13] B. Moore, S. Ghigna, F. Governato, G. Lake, T. Quinn, J. Stadel, and P. Tozzi, Astrophys. J. Lett. **524**, L19 (1999).
[14] G. Rhee, O. Valenzuela, A. Klypin, J. Holtzman, and B. Moorthy, Astrophys. J. **617**, 1059 (2004).

[15] P. Colín, V. Avila-Reese, and O. Valenzuela, Astrophys. J. **542**, 622 (2000).
[16] J. Sommer-Larsen and A. Dolgov, Astrophys. J. **551**, 608 (2001).
[17] P. Bode, J. P. Ostriker, and N. Turok, Astrophys. J. **556**, 93 (2001).
[18] C. Tao, in *CYGNUS 2011: Third International Conference on Directional Detection of Dark Matter*, EAS Publications Series Vol. 53 (Cambridge University Press, Cambridge, England, 2012), p. 97.
[19] R. Jeannerot, X. Zhang, and R. Brandenberger, J. High Energy Phys. 12 (1999) 003.
[20] W. B. Lin, D. H. Huang, X. Zhang, and R. Brandenberger, Phys. Rev. Lett. **86**, 954 (2001).
[21] S. Hannestad, arXiv:0008451.
[22] M. Fujii and K. Hamaguchi, Phys. Rev. D **66**, 083501 (2002).
[23] M. R. Lovell, V. Eke, C. S. Frenk, L. Gao, A. Jenkins, T. Theuns, J. Wang, S. D. M. White, A. Boyarsky, and O. Ruchayskiy, Mon. Not. R. Astron. Soc. **420**, 2318 (2012).
[24] X. Bi, R. Brandenberger, P. Gondolo, T. J. Li, Q. Yuan, and X. M. Zhang, Phys. Rev. D **80**, 103502 (2009).
[25] Y. Cui and D. E. Morrissey, Phys. Rev. D **79**, 083532 (2009).
[26] A. Lewis, A. Challinor, and A. Lasenby, Astrophys. J. **538**, 473 (2000).
[27] A. Boyarsky, J. Lesgourgues, O. Ruchayskiy, and M. Viel, Phys. Rev. Lett. **102**, 201304 (2009).
[28] J. F. Navarro, A. Ludlow, V. Springel, J. Wang, M. Vogelsberger, S. D. M. White, A. Jenkins, C. S. Frenk, and A. Helmi, Mon. Not. R. Astron. Soc. **402**, 21 (2010).
[29] J. Einasto, Trudy Inst. Astrofiz. Alma-Ata **5**, 87 (1965).
[30] R. Catena and P. Ullio, J. Cosmol. Astropart. Phys. 8 (2010) 004.
[31] P. Salucci, F. Nesti, G. Gentile, and C. Frigerio Martins, Astron. Astrophys. **523**, A83 (2010).
[32] M. Pato, O. Agertz, G. Bertone, B. Moore, and R. Teyssier, Phys. Rev. D **82**, 023531 (2010).
[33] S. Shao and L. Gao (work in progress).
[34] X.-J. Bi, M. Li, and X. Zhang, Phys. Rev. D **69**, 123521 (2004).
[35] J. A. R. Cembranos, J. L. Feng, A. Rajaraman, and F. Takayama, Phys. Rev. Lett. **95**, 181301 (2005).
[36] M. Kaplinghat, Phys. Rev. D **72**, 063510 (2005).
[37] A. V. Maccio, S. Paduroiu, D. Anderhalden, A. Schneider, and B. Moore, arXiv:1202.1282.
[38] J. Wang and S. D. M. White, Mon. Not. R. Astron. Soc. **380**, 93 (2007).
[39] J. F. Navarro, C. S. Frenk, and S. D. M. White, Astrophys. J. **490**, 493 (1997).
[40] S. Shao, L. Gao, T. Theuns, and C. S. Frenk, arXiv:1209.5563.
[41] Q. Yuan, X.-J. Bi, and J. Zhang, Chinese Phys. C **33**, 848 (2009).
[42] S. Hofmann, D. J. Schwarz, and H. Stöcker, Phys. Rev. D **64**, 083507 (2001).
[43] J. Diemand, B. Moore, and J. Stadel, Nature (London) **433**, 389 (2005).
[44] L. Gao, C. S. Frenk, M. Boylan-Kolchin, A. Jenkins, V. Springel, and S. D. M. White, Mon. Not. R. Astron. Soc. **410**, 2309 (2011).
[45] F. Donato, D. Maurin, P. Brun, T. Delahaye, and P. Salati, Phys. Rev. Lett. **102**, 071301 (2009).
[46] G. Jungman, M. Kamionkowski, and K. Griest, Phys. Rep. **267**, 195 (1996).
[47] S. Chatrchyan *et al.*, Phys. Rev. Lett. **107**, 221804 (2011).
[48] G. Aad *et al.*, Phys. Lett. B **710**, 67 (2012).
[49] E. Aprile *et al.*, Phys. Rev. Lett. **107**, 131302 (2011).
[50] G. Aad *et al.* (ATLAS Collaboration), Phys. Lett. B **716**, 1 (2012).
[51] CMS Collaboration, Phys. Lett. B **716**, 30 (2012).
[52] J. Ellis, T. Falk, K. A. Olive, and Y. Santoso, Nucl. Phys. **B652**, 259 (2003).
[53] H. Baer, A. Mustafayev, S. Profumo, A. Belyaev, and X. Tata, J. High Energy Phys. 7 (2005) 065.
[54] A. Djouadi, J.-L. Kneur, and G. Moultaka, Comput. Phys. Commun. **176**, 426 (2007).
[55] G. Bélanger, F. Boudjema, A. Pukhov, and A. Semenov, Comput. Phys. Commun. **176**, 367 (2007).
[56] G. Bélanger, F. Boudjema, A. Pukhov, and A. Semenov, Comput. Phys. Commun. **180**, 747 (2009).
[57] T. Sjöstrand, S. Mrenna, and P. Skands, J. High Energy Phys. 5 (2006) 026.
[58] A. W. Strong and I. V. Moskalenko, Astrophys. J. **509**, 212 (1998).
[59] R. Trotta, G. Jóhannesson, I. V. Moskalenko, T. A. Porter, R. Ruiz de Austri, and A. W. Strong, Astrophys. J. **729**, 106 (2011).
[60] O. Adriani *et al.*, Science **332**, 69 (2011).
[61] J. Liu, Q. Yuan, X.-J. Bi, H. Li, and X. Zhang, Phys. Rev. D **85**, 043507 (2012).
[62] A. D. Panov *et al.*, Bull. Russ. Acad. Sci., Phys. **73**, 564 (2009).
[63] H. S. Ahn *et al.*, Astrophys. J. Lett. **714**, L89 (2010).
[64] O. Adriani *et al.*, Nature (London) **458**, 607 (2009).
[65] J. Chang *et al.*, Nature (London) **456**, 362 (2008).
[66] F. Aharonian *et al.*, Phys. Rev. Lett. **101**, 261104 (2008).
[67] F. Aharonian *et al.*, Astron. Astrophys. **508**, 561 (2009).
[68] A. A. Abdo *et al.*, Phys. Rev. Lett. **102**, 181101 (2009).
[69] J. Zhang, Q. Yuan, and X.-J. Bi, Astrophys. J. **720**, 9 (2010).
[70] A. A. Abdo *et al.*, Phys. Rev. Lett. **104**, 101101 (2010).
[71] M. Ackermann *et al.*, Astrophys. J. **750**, 3 (2012).
[72] D. Hooper and L. Goodenough, Phys. Lett. B **697**, 412 (2011).
[73] W. B. Atwood *et al.*, Astrophys. J. **697**, 1071 (2009).
[74] R. Brandenberger and A. Riotto, Phys. Lett. B **445**, 323 (1999).
[75] M. B. Hindmarsh and T. W. B. Kibble, Rep. Prog. Phys. **58**, 477 (1995).
[76] R. H. Brandenberger, Int. J. Mod. Phys. A **09**, 2117 (1994).